Solid State Ionics 309 (2017) 100–109

Contents lists available at ScienceDirect

Solid State Ionics

journal homepage: www.elsevier.com/locate/ssi

High stability and ac-conductivity of cubic fluorite-Bi_2O_3 films synthesized by magnetron sputtering

Celia L. Gomez[a], Sandra E. Rodil[b,*]

[a] CINVESTAV-Unidad Queretaro, Queretaro 76230, Mexico
[b] Instituto de Investigaciones en Materiales, Universidad Nacional Autónoma de México, Mexico, Circuito exterior sn, Ciudad Universitaria, Ciudad de México 04510, Mexico

ARTICLE INFO

Keywords:
Doped bismuth oxide
Sputtering
Thin films
Impedance spectroscopy
Thermal stability

ABSTRACT

The electrical properties of nanostructured δ-Bi_2O_3 and doped Bi_2O_3 thin films are studied using electrochemical impedance spectroscopy. Firstly, it is shown that films presenting the cubic fluorite Bi_2O_3 phase can be stabilized in a wide temperature range by adding dopants; from room temperature to 300 °C for Al, 500 °C for Ta and 600 °C for W. An enhancement in the total mixed conductivity of about three orders of magnitude is obtained for the Al-doped films and only of two orders of magnitude for the other dopants in the low temperature range (100–250 °C). Impedance analyses suggest that the conductivity is predominantly driven by delocalized ion conduction occurring through the abundant grain boundaries of the nanostructured thin films.

1. Introduction

Solid-based electrochemical devices, such as solid oxide fuel cells (SOFCs), oxygen sensors, oxygen pumps and gas separation membranes requires the development of solid electrolyte materials with high ionic conductivity [1–3]. The defect fluorite phase (δ) of bismuth tri-oxide (Bi_2O_3) is the material that presents the highest ionic conductivity of 1–1.5 Scm^{-1} at 730–830 °C on bulk [4,5] compared to 0.01 Scm^{-1} for optimally doped YSZ at 760 °C. The high conductivity on the δ-Bi_2O_3 is due to the defective fluorite structure with ¼ of the anion sites empty [6]. The ionic conductivity is intrinsic of the δ-Bi_2O_3 structure, contrary to other ionic conductors where doping is required to obtain the high ionic conductivity. The δ-Bi_2O_3 is the stable phase at high temperature (730–825 °C) among the six polymorphs (α, β, γ, δ, ε and ω) of Bi_2O_3 [7,8]. However, bismuth oxide based materials present two major disadvantages, which are critical for their applications as solid electrolytes. Bismuth oxide has a low thermodynamic stability in reducing atmospheres; it can be completely reduced to metallic bismuth and it suffers volatilization at moderate temperatures [3].

The current demands on decreasing cost of SOFCs for example by reducing the operation temperature; which allows also the use of cheaper interconnects, and might improve the durability of the electrochemical devices, open an interesting opportunity window for the use of room temperature (RT) stabilized cubic δ-Bi_2O_3 [9]. A decrease in the working temperature and an increase in the oxygen partial pressures of the SOFCs bring bismuth oxide again to the candidate list of solid electrolyte materials. The stabilization of the cubic fluorite Bi_2O_3 phase at RT is actually done through substitution of Bi with isovalent (Y^{3+}, Er^{3+}, Dy^{3+}) and aliovalent (Ba^{2+}, Nb^{5+}, Ta^{5+}, W^{6+}) ion dopants during its preparation using solid-state reactions [10–15].

On the other hand, since 1999 [16], it was shown that the δ-Bi_2O_3 phase can be synthesized and kept stable at room temperature as thin films [17–21]; this has been achieved using different deposition techniques and substrates. The films are not structurally stable showing phase transformation and/or partial reduction at temperatures between 250 and 350 °C [17,22,23]. For intermediate temperature SOFCs, the films should be stable at least up to 500 °C [24]. The ionic conductivity measurements of bulk stabilized δ-Bi_2O_3 ceramics has been extensively reported demonstrating that in general the Arrhenius activation energy for oxygen migration increases and the conductivity decreases due to a rearrangement of the oxygen sublattice as a consequence of the dopant addition [6,25]. The use of double oxide dopants has been shown to be the best strategy to maximize the conductivity, since smaller amounts of dopants are required, reaching conductivities of 0.043 Scm^{-1} at 500 °C [26] or 0.098 Scm^{-1} at 500 °C [27].

Intents to stabilize the δ-Bi_2O_3 films and evaluate the ionic conductivity are still very rare. Wang et al. [28] deposited yttrium stabilized Bi_2O_3 (YSB) thin films on SiO_2 and MgO substrates using magnetron co-sputtering. The X-ray diffraction (XRD) patterns showed that the as-grown films were partially amorphous with a reflection around 28.14°, but after annealing at 500 °C they obtained the cubic δ-type phase. The ionic conductivity was studied using impedance

* Corresponding author.
E-mail address: srodil@unam.mx (S.E. Rodil).

http://dx.doi.org/10.1016/j.ssi.2017.07.007
Received 25 May 2017; Received in revised form 6 July 2017; Accepted 7 July 2017
Available online 24 July 2017

spectroscopy (IS) in a frequency range of 5 Hz–13 MHz from 400 to 800 °C with a planar configuration of cermet Ag-$(La_{0.7}Sr_{0.3})CoO_3$ electrodes. The Nyquist plot showed a semicircle at high frequencies related to the films resistance and a second one at low frequencies due to the electrodes resistance, however no details are given about the structural changes suffered by the films during the IS measurements. The results showed a change in the conductivity around 600 °C, probably associated to a phase transformation. The conductivity at 400 °C is about 9×10^{-4} Scm^{-1} and the authors claimed that it is similar to those reported for bulk YSB. Laurent et al. [29] reported the conductivity measurements of electrodeposited δ-Bi_2O_3 thin films on silver substrates in the 100–500 °C temperature range. The activation energy and conductivity values at 440 °C were comparable 0.35 eV and 0.39 Scm^{-1}. However, as the authors mentioned at 360 °C the films have already changed into a sillenite structure. More recently, Sanna et al. [30] deposited Er_2O_3 stabilized Bi_2O_3 (ESB) films by pulsed laser deposition (PLD) on different crystalline substrates. The films were highly oriented in the (111) plane associated with the cubic δ-type phase. The electrical characterization was performed using IS varying the amplitude signal from 500 mV to 2 V in a temperature range from 400 to 800 °C during heating and cooling cycles using gold paste electrodes on planar configuration. The conductivity values were much smaller (various orders of magnitude) than those reported for bulk ESB ceramics and the structure was strongly modified during the heating-cooling cycles. However, using a new approach; Sanna et al. [20,31] have been able to stabilize the PLD deposited δ-Bi_2O_3 phase at RT by confinement between other two fluorites. They [20,31] have shown that under this strong confinement Er-doped or undoped Bi_2O_3 can be stabilized and the hetero-structures (up to 20 nanolayers) lead to ionic conductivities (~0.055 Scm^{-1} at 550 °C and ~0.32 Scm^{-1} at 650 °C) comparable to the δ-Bi_2O_3 which remains stable for long periods (100 h).

In our previous work [23], we demonstrated that by the addition of Ta ions, it was possible to keep the δ-type phase up to 500 °C in sputtered deposited Bi_2O_3 thin films. In that paper, however, we did not include conductivity measurements. The aim of the present work is to introduce the effect of introduction of cations with different size and valence (Al^{3+}, W^{6+}, Ta^{5+}) on the thermal stabilization of the defect fluorite structure of the Bi_2O_3 thin films and report their transport properties. The conductivity of the non-doped Bi_2O_3 and doped Bi_2O_3 thin films were characterized using impedance spectroscopy within the temperature range where the defect fluorite phase was maintained.

2. Experimental details

The deposition of the Bi_2O_3 and doped Bi_2O_3 thin films was done using magnetron sputtering in an O_2:Ar (20:80) reactive atmosphere, 100 W rf power, 10 min deposition time, substrate-target distance 5 cm, base pressure below 6.7×10^{-4} Pa, and deposition pressure 3.9 Pa; the deposition parameters were based on our previous work [32]. However, for the doping, small variations in the substrate temperature (Table 1) were adjusted in order to obtain the cubic fluorite phase. The doping was done using tantalum wires (210 mm^2), tungsten plates (510 mm^2) or aluminum plates (510 mm^2) attached to the α-Bi_2O_3 target (4″), and this allows the deposition of uniform and homogeneous films within a 2″ × 2″ area. Since the films were grown under the Ar/O_2 reactive atmosphere, it is expected that during the film growth the metallic pieces are completely ionized, so we are really adding metal oxides into the growing Bi_2O_3 films.

Table 1
Substrate temperature and area of the dopant attached to the α-Bi_2O_3 target. Valence and ionic radii of the dopants.

Sample name	Sample	Dopant (area)	Valence	Radii/nm	Substrate temperature/°C
Bi_2O_3	Bi_2O_3	–	3 +	9.6	125
WBO	Bi_2O_3:W	W plates (510 mm^2)	6 +	6.2	210
TaBO	Bi_2O_3:Ta	Ta wire (210 mm^2)	5 +	6.8	125
AlBO	Bi_2O_3:Al	Al plates (510 mm^2)	3 +	5.1	210

The films were deposited on glass substrates; the structure was characterized by X-ray diffraction using a Rigaku Ultima IV diffractometer with the CuKα radiation in the thin film mode (incident parallel beam) from 20 to 60°. The thermal stability of the films in air was evaluated by heating the XRD stage from RT to 600 °C at a heating speed of 10 °C/min. The films were allowed to stabilize at each temperature step (50 °C) during 30 min before acquiring a new XRD pattern.

The micrographs of the films surface were obtained using a Field Emission-Scanning Electron Microscope (JEOL7600F FE-SEM) at 2.0 kV with an EDX detector (Oxford) to evaluate the dopant concentration. The film thicknesses were measured by a Dektak profilometer on a step left on purpose during the deposition. Rectangular aluminum electrodes of 0.8 cm of width, 1.2 cm of length and 0.8 cm of separation were evaporated on the film surface for in-plane characterization. The conductivity of the electrolyte thin films was determined by impedance spectroscopy using a Gamry Reference 600 potentiostat with 1 V of signal amplitude and a frequency range from 1 Hz to 1 MHz (temperature range from RT to 250 °C). The measurements were done by triplicate (three films deposited together) to confirm the reproducibility. The spectra were fitted to a standard RC_{cpe} circuit to obtain the resistance (R) and then converted to conductivity using the equation

$$\sigma = \frac{1}{R}\frac{t}{ab} \quad (1)$$

where *ab* is the area between the electrodes and *t* the film thickness. The impedance spectra were also analyzed using the imaginary part peaks (Z″ vs f plots) to evaluate the relaxation frequency as a function of the temperature. Activation energies for the conductivity (σ) and the hopping frequency were obtained from analysis of the corresponding Arrhenius plots.

3. Results

3.1. Microstructure and composition

Fig. 1 shows the XRD patterns of the Bi_2O_3 and the doped films: TaBO, AlBO and WBO at three different temperature values; room temperature (RT), 250 °C, which is the maximum temperature used for the electrical characterization and the limit temperature at which the cubic fluorite phase could be maintained depending on the doping.

For all the samples, the RT-XRD patterns show the five characteristics peaks of the cubic δ-Bi_2O_3 (ICDD-00-052-1007). The relative intensity between the diffraction peaks is very similar to that expected for a powder sample, indicating that non-preferred orientation was established, contrary to XRD patterns reported by other authors [33,34]. The XRD data do not show the presence of segregated oxide phases (TaO_x, AlO_x or WO_x) or formation of ternary oxides; the XRD data suggest the formation of single phase cubic δ-type Bi_2O_3 films with a minor reduction in the lattice parameter indicative of the formation of solid solutions [10]. The lattice parameters were reduced from 0.55428 nm of the Bi_2O_3 film to 0.553986, 0.55374, 0.52918 nm for the AlBO, WBO and TaBO samples, respectively, such reduction is in agreement with the lower ionic radii of the dopants since the Bi substitution will reduce the lattice parameter. However, XRD cannot show the superstructures which have been identified for the bulk Bi_2O_3-M_2O_3 systems [10,11]. The crystalline domain size of the Bi_2O_3 and doped Bi_2O_3 was obtained using the PDXL2 software and the Halder-Wagner method [35] which is more precise than the typical Scherrer method. For the as-deposited

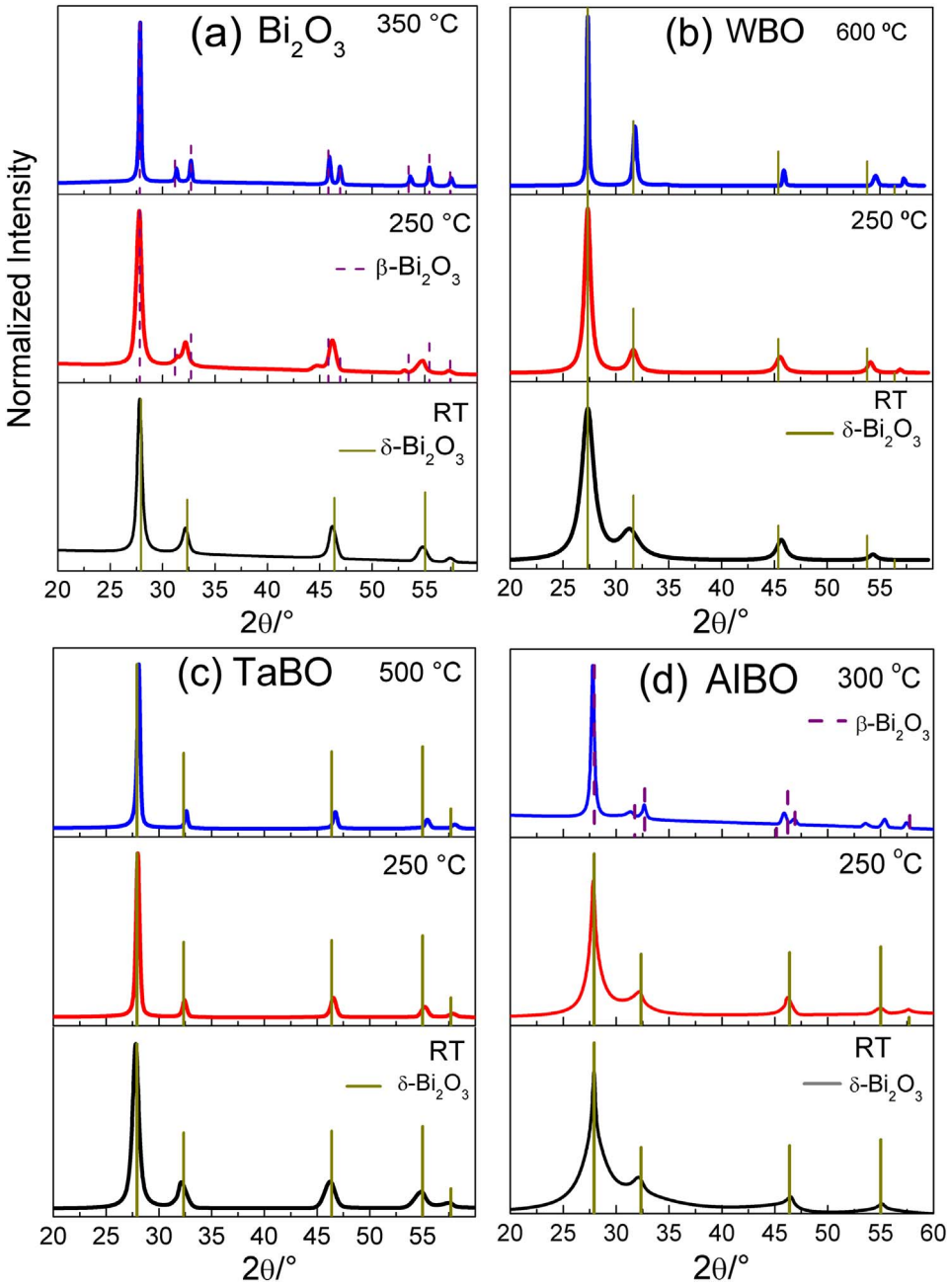

Fig. 1. XRD patterns of the undoped and doped bismuth oxide films obtained in the high temperature stage of the diffractometer. Lower panel refers to the room temperature (RT) patterns, middle panel shows the structure of the films at 250 °C and top panel shows the maximum stability achieved.

Table 2
Thickness, crystalline domain size obtained by Halder-Wagner method, atomic percentage of the dopant from the EDS analysis.

Sample	Thickness/nm[a]	Crystallite size/nm[b]	Doping/at.%[c]
Bi_2O_3	346 ± 35	11 ± 1	–
WBO	235 ± 24	18 ± 1	3.1 ± 0.4
TaBO	178 ± 18	9 ± 1	8.4 ± 0.2
AlBO	215 ± 22	15 ± 1	2.1 ± 0.2

[a] Standard deviation from measurements on different sample positions lead to an error of about 10%.
[b] Half the maximum domain size that can be estimated.
[c] Standard deviation from different measurements.

films, the XRD patterns indicated that the samples are nano-crystalline with grain sizes in the 9–18 nm range, without any trend related to the dopant, as shown in Table 2.

Fig. 1 also shows the diffraction patterns obtained after annealing the samples for 30 min in the XRD heating stage (The XRD patterns were obtained every 50 °C but not all temperatures are shown for clarity). At 250 °C, it can be observed that only the Bi_2O_3 samples has already started a transformation into the beta-phase, which at 350 °C is clearly formed (top Fig. 1(a)). The other three samples; TaBO, WBO and AlBO remained nearly unchanged at 250 °C; only changes in the peak width are observed. The top XRD patterns for the W (Fig. 1(b)) and Ta (Fig. 1(d)) doped samples show the maximum temperature at which the delta-type phase could be stabilized; 600 and 500 °C, respectively. Finally, not such a large stability was obtained when Al was used as a dopant; the diffraction pattern of the AlBO sample after annealing at 300 °C (Fig. 1(b) top), already showed peaks related to the beta-phase. As expected, the crystalline domain size increased with the annealing, but the values were still in the nanometric range; between 30 and 90 nm.

Fig. 2 shows the SEM images of the as-deposited samples, where it can be observed that the surface topography is composed of small grains larger than the average crystalline domain. The size distribution

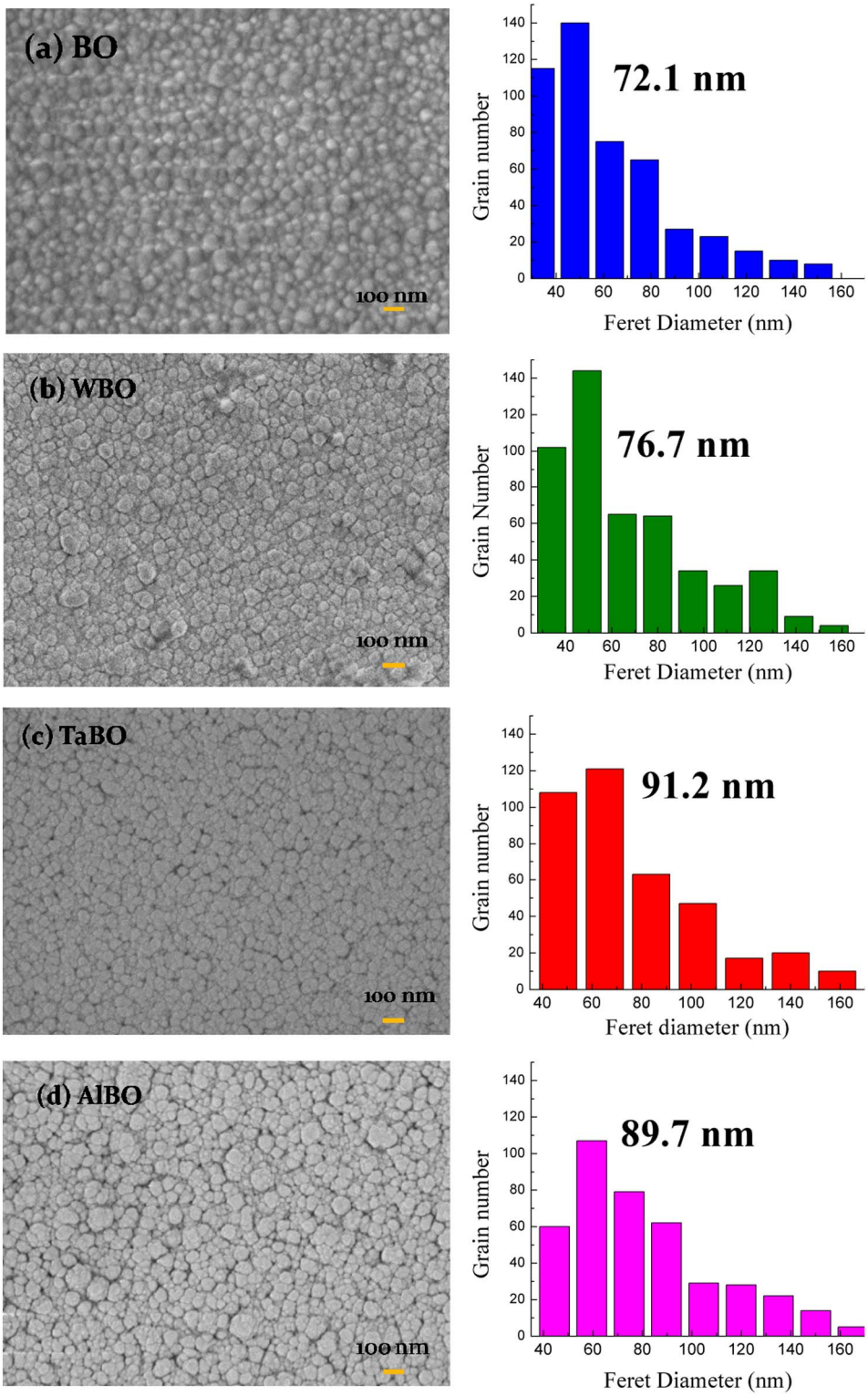

Fig. 2. Front view of the samples surface by SEM using low electron voltage (5 keV) to avoid charging effects. The distribution of the average grain size (Feret diameter) is shown for each sample (a) Bi_2O_3, (b) WBO, (c) TaBO and (d) AlBO.

of these grains is shown for each figure in terms of the Feret diameter and the media values ranged between 70 and 90 nm. The EDX technique was used to estimate the atomic percentage of the dopant thorough the film thickness. The values reported in Table 1 correspond to the average value obtained from at least 4 different zones with their respective standard deviation (s). For each dopant, the number of wires or plates attached to the Bi_2O_3 was changed and here we reported only the condition at which we were able to obtain the cubic fluorite phase for as-deposited samples. The amount of dopant concentration that allowed the structural stabilization of the δ-type Bi_2O_3 phase was different in each case. For the TaBO samples, the cubic phase was obtained when the dopant concentration was 8.4 at.%, attained using two Ta (1 mm diameter) wires attached to the target, however, when only one wire was used, the Ta content was not reliably detected by EDX. For WBO, the dopant concentration was 3.1 at.% using three small W pieces (5 × 0.25 mm), when two pieces were used the W concentration was 2.7 at.%, and the thermal stability was 500 °C. Finally, for the AlBO, only a single piece (5 × 5 mm) was attached and it was already difficult

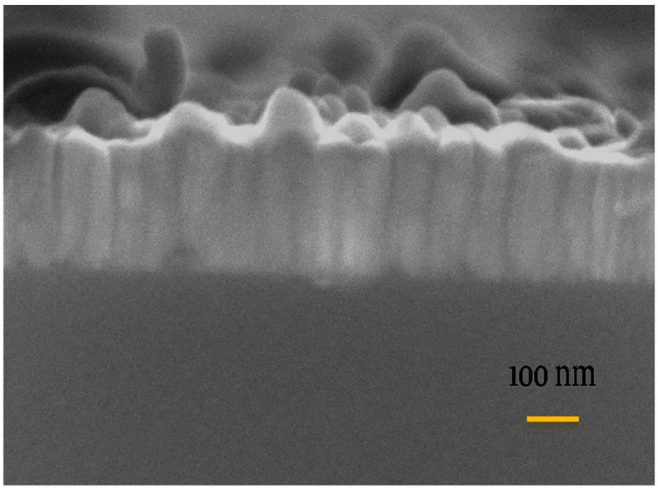

Fig. 3. Representative SEM cross-section image of the Bi_2O_3 film. The doped films presented a similar morphology.

to get the phase without increasing slightly the substrate temperature, reaching an Al concentration in the films of 2.1 at.%. At the reported dopant concentrations, the XRD data shows that is possible to accommodate the metal cations preserving the fcc atom array of the fluorite structure [10]. Apart from Bi, O and the dopant, no other elements were detected by EDX in these films.

The incorporation of the dopant into the bismuth oxide thin films using magnetron sputtering with a single-compose target is dependent on the area and positioning of the metallic piece, their sputter yield and it will also be determined by the solubility of the metal into the Bi_2O_3 structure. Therefore, under this configuration it was not possible to perform a concentration-dependence analysis of both the structure and the electrical properties. Further works will involve the co-deposition using separate targets in order to achieve a better control of the dopant concentration. However, as observed in the XRD data, we have proved that it is possible to widen the stability temperature range of the δ-type Bi_2O_3 thin films using different dopants. Previously, the maximum temperature to keep the cubic-fluorite phase of Bi_2O_3 thin films was 250 °C for our samples [23] and 350 °C by other authors [22].

Fig. 3 shows the cross-section image of the undoped Bi_2O_3 film, where the typical columnar growth of sputtered samples can be observed. All films presented a very similar morphology. The width of such columns is below the 100 nm and not large voids between them are observed; the films presented a dense microstructure.

3.2. Electrical properties

The impedance spectra of the four samples were obtained only within the temperature of maximum stability for the cubic fluorite Bi_2O_3 samples (δ-Bi_2O_3 type phases), i.e. from room temperature to 250 °C. The measurements below 100 °C showed strong influences from the adsorbed species on the sample surface and this was confirmed by doing hysteresis cycles, so those data are not included in the analysis.

Fig. 4 presents the impedance plots of Bi_2O_3 and doped Bi_2O_3 films between 100 and 250 °C. It can be clearly observed that they are characteristic of a single semicircle, which radii rapidly decreased as the temperature was increased for all samples. As far as the sample was heated to the measurement temperature and maintained for more than 20 min before initiating the acquisition of the data, the impedance spectra did not change after 4 consecutive measurements suggesting a good stability of the conductivity (S1). As it has been reported previously [36], for nanometric grain size materials, there is a strong overlap between the grain and grain boundary contributions which lead to a single semicircle [37,38]. The effect of the electrode is not observed, probably because under the used geometrical design of the electrodes, the electrode resistance is small compared to the samples resistances. In such case, only the total resistance can be obtained and this was done using a parallel RC_{cpe} equivalent circuit; a constant phase element was used instead of a capacitor to take into account the depressed semicircles [39,40].

From the total resistance, the film conductivity can be estimated and the corresponding Arrhenius plots are shown in Fig. 5, where it can be observed that the ac-conductivity at 250 °C change depending on the dopant following the trend Bi_2O_3 (4.2×10^{-6} Scm^{-1}) < WBO (2.1×10^{-4} Scm^{-1}) ≈ TaBO (3.1×10^{-4} Scm^{-1}) < AlBO (5.1×10^{-3} Scm^{-1}). However, at low temperature (100 °C), only the AlBO sample showed a relative higher conductivity (two orders of magnitude higher than the other samples). The activation energies (ΔE_c) are reported in Table 3 and are comparable to values reported for the stabilized δ-type Bi_2O_3 ceramics [41–43].

A comparison of the ac-conductivity versus temperature of the films with data taken from the literature concerning doped-ceria [44–47] and doped-zirconia [48–50] thin films using similar configuration of electrodes than in this work, can be observed in Fig. 6, which also contains data from heavily doped ceria nanoceramics [36]. It can be observed that the conductivity obtained for doped δ-type Bi_2O_3 films, although was only measured at low temperature (100–250 °C) to ensure the structural stability, is relatively higher than all other materials and interesting larger than heavily doped ceria nanoceramics [36] measured in the same temperature range. The conductivity values obtained for the films are lower than those reported for the δ-Bi_2O_3 high temperature phase that reach conductivities of 1.8 Scm^{-1} above 750 °C [51] but are not far from the conductivities reported at 500 °C for dopant stabilized bismuth oxide ceramics (4.2×10^{-2} to 4.6×10^{-4} Scm^{-1}) [3,43,51] and also close to the recent values obtained for heterostructurally-stabilized δ-Bi_2O_3 (~5.5×10^{-2} Scm^{-1} at 550 °C) [31]. However, we will need to perform measurements at higher temperatures, at least the 450–550 °C range where most of the data is reported in order to confirm the predictions from the "σ vs. T" trend observed in Fig. 5.

The high values of conductivity in combination with the low conductivity activation energies, ΔE_c for these nanometric and dense thin films, suggested that the electrical (ionic or mixed) transport is determined by the interfaces and grain boundaries. Kosacki et al. [52] have shown that for nanostructured ceria or zirconia samples, there is an increment in the conductivity by two or three orders of magnitude and a decrease in the activation energy. This has been explained in terms of the more important role played by the grain boundary diffusion, which is larger than in the grain interior and becomes dominant for nanostructured materials due to the larger volume fraction of grain boundaries. Similarly, for doped ceria nanoceramics the enhancement on the ionic conductivity at low temperatures (125–150 °C) as the grain size was decreased in the 35–50 nm range have been demonstrated by Bellino et al. [36]. These authors proposed that the ionic transport in these nanoceramics occurs via the oxygen vacancies placed at the grain boundaries that act as the delocalized carriers [53]. For yttria doped zirconia films deposited by magnetron sputtering, it has also been demonstrated that larger ionic conductivity can be achieved on the nanometric thin films at relative lower doping level than for YSZ bulk material [54]. Furthermore, the increased conductivity obtained by Sanna et al. [31] for the Bi_2O_3/YSZ heterostructures as the number of interfaces increased has been explained in terms of the enhanced mobility of the charge carriers at the interfaces [55–57].

The temperature dependence of the relaxation processes in the films were obtained from plotting the imaginary impedance versus the frequency (Z″ vs f), where the characteristic frequency correspond to the value at which Z″ is maximum (Fig. 7). For the four samples, a single Debye-like peak [58] can be observed whose maxima shifts to higher frequencies as the temperature was increased. The higher frequencies in the whole temperature range correspond to the Al-doped bismuth oxide. Meanwhile for the other samples there is a different behavior at

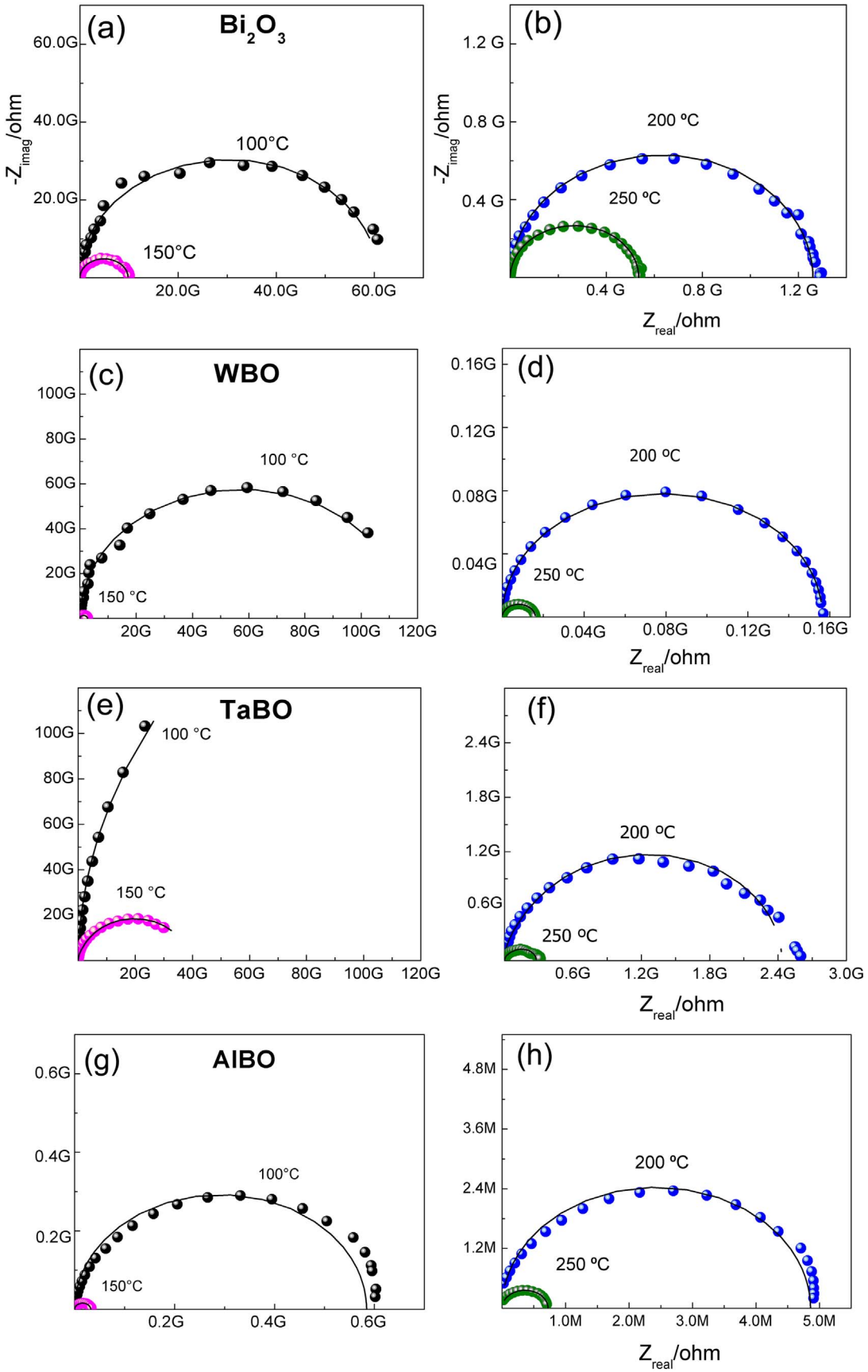

Fig. 4. Nyquist diagram of the electrochemical impedance data for the doped and undoped films. (a) Bi_2O_3, (b) WBO, (c) TaBO and (d) AlBO; the top panel shows measurements at 100 and 150 °C and the lower panel includes the 200 and 250 °C data. Since the radii of the decreased rapidly as the temperature is increased, the two ranges has to be shown separately.

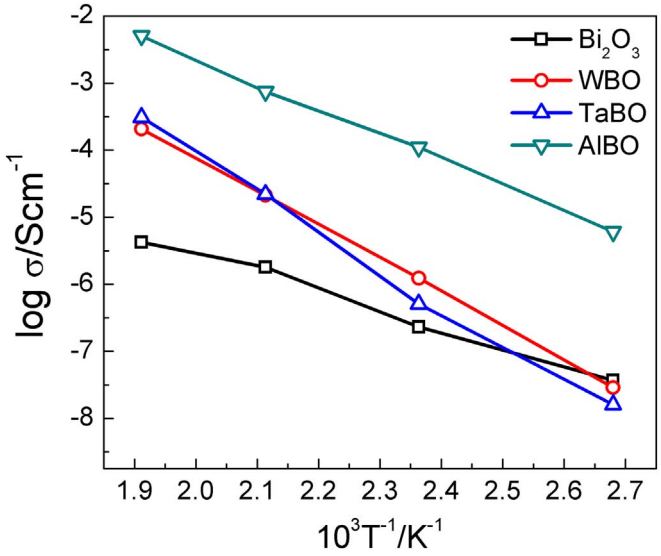

Fig. 5. Arrhenius representation of the conductivity measurements for all samples.

Table 3
ac-Conductivity (σ) measured at 250 °C and the conductivity activation energy (ΔE_c). Value of the peak frequency (f_h) obtained from the Z″ vs. f plot and the hopping activation energy (ΔE_h). The activation energies were obtained from the corresponding Arrhenius plots.

Sample	Doping/at.%	σ/Scm^{-1} 250 °C	ΔE_c/eV	f_h/kHz 250 °C	ΔE_h/eV
Bi_2O_3	–	4.2×10^{-6}	0.55	0.6	0.50
WBO	3.1 ± 0.4	2.1×10^{-4}	0.99	20	1.00
TaBO	8.4 ± 0.2	3.1×10^{-4}	1.12	20	1.13
AlBO	2.1 ± 0.2	5.1×10^{-3}	0.75	251	0.70

100 °C than at 250 °C; at the low temperature, the Bi_2O_3 sample shows a larger frequency than the WBO and TaBO samples. However, at 250 °C, the peak frequencies for WBO and TaBO are alike and one order of magnitude larger than the pure Bi_2O_3 film. Assuming the simplest of the conduction models (non-dispersive conductors) [58,59], where the conductivity is visualized as a series of independent hop of ions over potential barriers along the direction of the applied electric field, the Z″ peak frequency is related to a fundamental ionic hopping mechanism, which is thermally activated. The frequency values obtained in this work are similar to those reported by Laukaitis et al. [48] for YSZ films in the corresponding temperature range.

The activation energies for the hopping process (ΔE_h) were obtained from the slope in the log(peak-frequency) vs 10^3/T Arrhenius plots shown in Fig. 8 for all samples. The hopping activation energy values (Table 3) are very similar to the activation energies of the conductivity (ΔE_c), suggesting that the increment in the conductivity with temperature is related to a larger probability of hopping through vacancies. According to Orliukas et al. [60,61], the fact that both activation energies are alike is an indication that the concentration of charge carriers remains constant within the studied temperature range and the conductivity is due to the jumping of mobile ions to vacant lattice sites under the influence of the electric field.

4. Discussion

Previous papers have clearly demonstrated that the δ-Bi_2O_3 structure, which possesses a high ionic conductivity, can be obtained at RT using thin film deposition methods [16,17,21,22,32]. However, the structure is lost when the sample is heated above 250–350 °C [17,22,23] and so far very few studies about the ac-conductivity of these films have been reported [28–30].

The current paper has two objectives; firstly to show that it is possible to enlarge the structural stability range of the sputtered δ-Bi_2O_3 thin films using different dopants and secondly, to report the transport properties of the films measured by impedance spectroscopy in the low temperature regime, aiming to their use for intermediate temperature micro SOFCs.

4.1. Stabilization of the δ-Bi_2O_3 phase

In the bulk phase, the stabilization of the δ-type Bi_2O_3 structure down to room temperature by doping with metal ions (M) having different radius can be simply explained in terms of the thermodynamics stabilization. A very clear description of the process was given by Meng et al. [26]. The addition of Metal-Oxygen (M-O) bonds with different lengths and strength than the Bi—O bond into the highly symmetric cubic structure stable above 730 °C means that when the temperature is decreased, the structural change into a lower symmetric structure (tetragonal-β or monoclinic-α) would be accompanied by a large negative entropy change associated to breaking apart or deforming the stronger M-O bonds. Therefore, addition of M-O bonds allows the thermodynamic stabilization of the defect fluorite Bi_2O_3 structure, but it typically affects negatively the ionic conductivity. For the Bi_2O_3, the ionic conductivity is decreased and the activation energy is increased since the stronger M-O bonds induce localization of the O vacancies; O

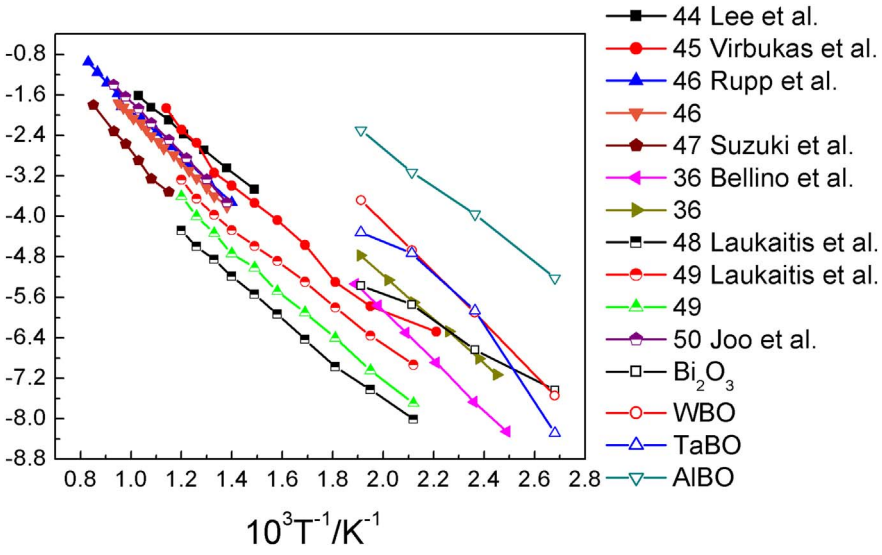

Fig. 6. Comparison of the variation in the ac-conductivity with the inverse of the temperature between the samples produced in this work (open symbols), ceria stabilized nanoceramics and both ceria and zirconia stabilized thin films.

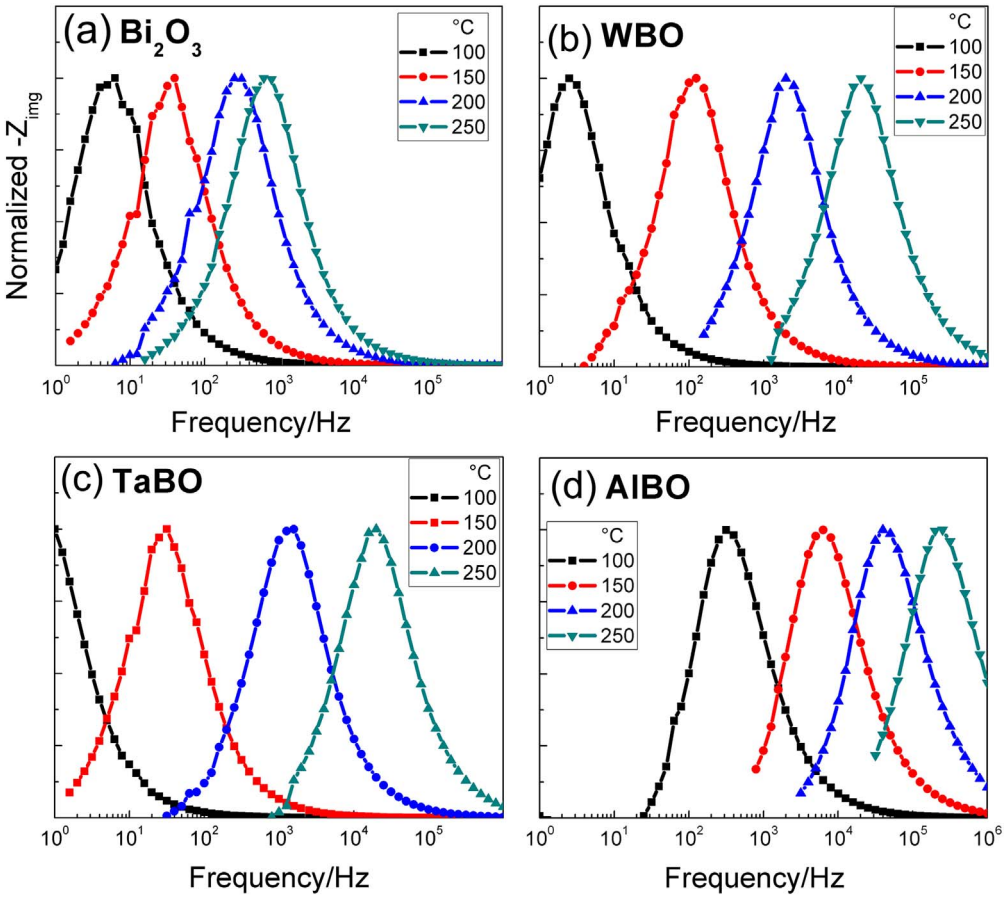

Fig. 7. Normalized Z″ versus frequency plot. The Z″ value is scaled by the resistivity (real impedance) of the samples, so their actual intensity changes with temperature. However, to show that there is a Debye-like peak shape for all temperatures and samples, the normalized data is presented.

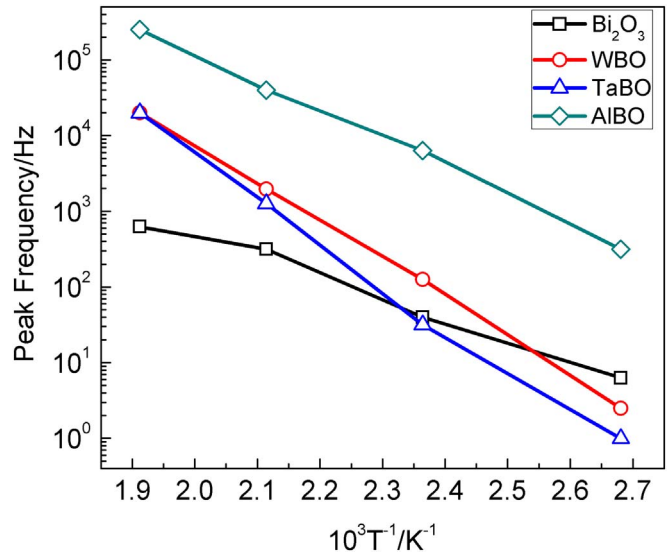

Fig. 8. The variation of the peak-frequency follows an Arrhenius dependence with the temperature, from which the corresponding hopping frequencies were estimated.

ions can participate in the electrical conductivity only after the M-O bonds are broken.

For the thin films, the δ-Bi_2O_3 phase can be obtained and kept at room temperature without doping. As explained in a previous paper [34], one of the possible explanations for the synthesis of metastable cubic Bi_2O_3 films is based on the kinetic effect of particle size that was proposed for the stabilized zirconia. For the ZrO_2 [62], it has been observed that when the crystalline size is below a critical value, the larger surface energy of the monoclinic phase in comparison to the tetragonal one prevents the transformation into the monoclinic phase. Such model has not been verified for the Bi_2O_3 films, but in most cases, the delta-phase has been obtained for nanocrystalline thin films. And this model will explain that when the annealing temperature is increased, and so does the crystallite size, the minimum particle size condition is no longer valid, and the films start the transformation into more thermodynamically stable phases. However, the mechanism by which the dopants allow the stabilization of the metastable cubic fluorite δ-type Bi_2O_3 phase is not clear. We have shown above, and in our previous paper about the TaBO films [23], that adding the dopants do not inhibit the growth of both the crystalline domains and grains and nevertheless, for Ta and W, it was possible to keep the cubic phase up to 500 and 600 °C, respectively. Despite that the stabilization of the δ-type Bi_2O_3 thin films cannot be explained in terms of the thermodynamics restrictions, the results agree with the previous reports about the stabilization of the delta-type phases using M_2O_3 oxides in the bulk [10,11,63]. These authors [10,11,13,63] have studied the quenching of the cubic fluorite-Bi_2O_3 phase to room temperature by adding transition metal oxides; such as Nb_2O_5, Ta_2O_5, WO_3 and MoO_3, finding that it is possible to obtain fluorite-like solid solutions of those systems, as far as the M_2O_3 concentration remains below 25 mol%. Then for Ta, solid solutions can be obtained up to 9 at.% and for W, up to 5.25 at.%. Nevertheless, both authors [10,11,13] agree that the structure is not purely defect fluorite, since the metal atoms present certain order dictated by the ordering of the oxygen vacancy array, so different types of structures were distinguished. Ling [10] also suggested that charge valence (5 + or 6 +) of the guest cation is more relevant than cation size to stabilize the delta-type structure but limited to concentrations below 25 mol%, which is exactly what has been observed in this study.

The W^{6+} dopant with a similar ionic radius (0.62 Å) than Ta^{5+} (0.68 Å) and slightly larger than Al^{3+} (0.51 Å) was more effective on stabilizing the fluorite structure, reaching the 600 °C without any signal of oxide reduction or structural variations. Nevertheless, as mentioned above the consequence of using high valence dopants is that the oxygen vacancies are reduced and therefore it would not be as good for the ionic conductivity.

4.2. AC conductivity

The conductivity measurements showed that the mixed ac-conductivity increased for the doped films in comparison to the pure Bi_2O_3 film, not in complete agreement with the results from the bulk phase, where ac-conductivity is usually reduced for bismuth oxide [51]. The activation energy for conductivity was increased indicating that similar to the bulk phase, there is a degree of localization of the vacancies around the dopants or as described by Battle et al. [6], and more recently by Wachsman [25], there is a rearrangement of the oxygen sublattice associated to the fluorite Bi_2O_3 structure around the dopant.

Increase in the ac-conductivity of bulk doped Bi_2O_3 ceramics have only been observed in few occasions. Meng et al. [26] showed that by using two oxide dopants instead of single-dopant, it was possible to decrease the content of the dopants to stabilize the fluorite phase at RT resulting in a slight increase in the conductivity. The stabilization was attributed to the entropy increase in the ternary system due to the presence of two different oxides while the increase in the conductivity to the lower content of the dopants, which allows a larger relative content of Bi atoms with higher polarizability. Similarly, Jung et al. [27,64] have also demonstrated that by co-doping (Dy and W) with precise dopant concentrations, it was possible to enhance the long-term stability of δ-Bi_2O_3 bulk materials, keeping the conductivity as high as 0.0068 Scm^{-1} at 500 °C for 500 h without phase and structural variations. Meanwhile, Jiang et al. [43] have also shown that Dy and W double doping at low molar concentrations (11–17%) lead to high ionic conductivity 0.043 Scm^{-1} at 500 °C and low activation energies of 0.47 eV.

For other ionic conductors, such as CeO_2 or ZrO_2, dopants are required to increase the conductivity since the oxygen vacancies are introduced to compensate the charge when trivalent cationic oxides are introduced (M_2O_3), so even in heavily doped samples, the ionic conductivity is enhanced by doping. For the fluorite Bi_2O_3, dopants can occupy the intrinsic vacancies instead of generating new ones and depending on the valence, excess electron or holes could be introduced. In this work, the stabilization of the cubic fluorite phase to intermediate temperatures was obtained using cations of higher valence than Bi^{3+}; W^{6+} and Ta^{5+}, so it is possible that these dopants which dissolve substitutionally in the oxide result in an increase in the concentration of electrons and/or a decrease in the concentration of oxygen vacancies, in agreement with the higher stabilization temperature. The bulk results indicated that valent 5 + and 6 + cations substituted Bi^{3+} reducing the number of available fluorite type oxygen vacancies [10,11,13]. Therefore, it is possible that the increase ac-conductivity for the TaBO and WBO films is due to an increase in the electronic conductivity. In order to confirm this, conductivity measurements versus the partial pressure of oxygen need to be performed. Here it should be mentioned that a mixed electronic-ionic conductor is currently considered an advantage for solid electrolyte fuel cells than a purely ionic conductor [2,65]. In terms of the efficiency, the mixed ionic-electronic electrolyte is preferred as far as it has a higher ionic conductivity than a purely ionic conductor.

The results for the AlBO samples are different since Al is isovalent to Bi, suggesting that if Al^{3+} is dissolve substitutionally, the electronic density will not be affected. It is more common that doping of M_2O_3 oxides with divalent or trivalent oxides lead to the creation of oxygen vacancies. Therefore, despite this dopant did not improve significantly the thermal stability of the cubic fluorite Bi_2O_3 structure, it becomes worth of further investigation due to the large enhancement observed for the ac-conductivity. It is important to notice that the Al dopant concentration was the smallest in comparison to the other dopants, which may have an impact in both the thermal stability and the transport properties.

It is also important to consider the works about the effect of the oxygen sublattice ordering on the conductivity of the defective fluorite δ-type Bi_2O_3 material [25]. Aidhy et al. [66] have found by molecular dynamic simulations that ordering of the anion vacancy sublattice limits the oxygen diffusivity, while experimentally [67] it was found that ordering lead to higher activation energies. Moreover such ordering, which is common in fluorite oxides at high vacancy concentrations depend on dopant radii and polarizability. According to this, the ideal dopant to improve conductivity of bismuth oxide should have similar ionic radii and polarizability than the Bi^{3+} [25]. However, the disadvantage is that when the difference in radii between Bi and the dopant is too small, the fluorite structure cannot be stabilized [41]. It was also showed that by doping with less polarizable lanthanides elements, the extent of short-range vacancy ordering increases and therefore the ionic conductivity decreases with increasing concentrations, so the smallest dopant concentration should be used. Considering the dopants used in this work, we see that the dopant radii follows the relations Bi^{3+} (0.96 Å) > Ta^{5+} (0.68 Å) > W^{6+} ion (0.62 Å) > Al^{3+} (0.51 Å) i.e. the polarizability [68] of the dopants are reduced in comparison to Bi^{3+} but also the dopant concentration follows the same relation Ta at.% > W at.% > Al at.%. Therefore, the larger conductivity and lower activation energy observed for the AlBO compared to WBO and TaBO might be explained as a consequence of the lower dopant concentration.

The ac-impedance spectra were dominated by a single semicircle which is normal for nanostructured materials, the consistency of the data was evaluated by doing a Kramers-Kronig analysis. From the circuit analysis, we were able to obtain the ac-conductivities which are considerable higher than those reported for doped-ceria or doped-zirconia nanoceramics reported in the same temperature range as this work (100–250 °C) [36], as shown in Fig. 6. The measurements for doped ceria [44–47,52,69] or zirconia [48,50,54] thin films are usually reported in a higher temperature range, so the conductivity values cannot be directly compared but assuming a linear extrapolation of the data shown in Fig. 6, the conductivity values obtained in this work are comparable or even larger than other films. The high conductivities are probably associated to the reduced grain sizes and abundance of grain boundaries in these nanostructured bismuth oxide thin films. Therefore, the classical models to explain the conductivity for bulk polycrystalline ceramics, such as the brick-bulk layer model, cannot be applied, as it has been shown for nanostructured ceramics [53]. The role of the interfaces in the ionic conductivity has also been demonstrated for bismuth oxide films or other ionic conductors, showing that it is possible to enhance the charge carrier transport by increasing the interfaces [31,55,56].

The analysis of the ac data using the impedance formalism showed a Debye-like behavior for all films, whose relaxation frequencies were thermally-activated with activation energies similar to the conductivity values. This similarity is an indication that the concentration of charge carriers remains constant within the studied temperature range and the conductivity is due to the jumping of mobile ions to vacant lattice sites under the influence of the electric field [61]. Moreover, following the idea of Bellino et al. [53] such ionic oxygen hopping is possibly occurring through the grain boundaries.

On the other hand, because we are reporting the conductivity at low temperatures (100–250 °C) we cannot exclude the contributions from proton conduction to the measured conductivity values. Proton conduction has been demonstrated for both thick-porous and thin-dense solid ionic conductor films [70–73], therefore further analysis of the conductivity on these Bi_2O_3 films under wet and dry ambient conditions are required to determine the possible contribution of proton conduction.

5. Conclusions

Pure bismuth oxide and doped-bismuth oxide films were deposited by magnetron sputtering. The as-deposited films presented the cubic delta phase with crystalline domains below 20 nm agglomerated forming a columnar dense structure with diameters in the 70–90 nm range. Dopants with different ionic radii, valence and concentrations were used; Al^{3+}, Ta^{5+} and W^{6+} with the purpose of increasing the thermal structural stability of the films. It was shown that Al (2.5 at.%) allows the stabilization of the δ-Bi_2O_3 type phase up to 300 °C, but lead to the higher increase in the conductivity (in the whole temperature range 100–250 °C range); attaining three order of magnitudes above the Bi_2O_3 films. The other dopants; Ta (8.4 at.%) and W (3.2 at.%) were more effective for the film structural stabilization, up to 500 °C and 600 °C, respectively. However, the conductivity was less enhanced and only at higher temperatures. Analysis of ac data in terms of the impedance formalism ($-Z''$ vs log(f)) allow us to propose that the main transport mechanism for all films is through ionic hopping, which presented a hopping activation energy very similar to the activation energy for the conductivity.

Acknowledgements

The research leading to these results has received funding from the European Community Seven Framework Programme (FP7-NMP-2010-EU-MEXICO), CONACYT (BisNano) under grant agreements No. 263878 and 125141, respectively and CONACYT 251279 project. CLG acknowledges CONACYT for the PhD scholarship. The authors acknowledge the technical support from A. Tejeda for XRD measurements, O. Novelo and J. Romero for SEM images and H. Zarco for technical support.

References

[1] S.C. Singhal, Solid State Ionics 135 (1–4) (2000) 305.
[2] S.M. Haile, Acta Mater. 51 (19) (2003) 5981.
[3] A.M. Azad, S. Larose, S.A. Akbar, J. Mater. Sci. 29 (16) (1994) 4135.
[4] H.A. Harwig, A.G. Gerards, Thermochim. Acta 28 (1) (1979) 121.
[5] N.M. Sammes, G.A. Tompsett, H. Nafe, F. Aldinger, J. Eur. Ceram. Soc. 19 (10) (1999) 1801.
[6] P.D. Battle, C.R.A. Catlow, J. Drennan, A.D. Murray, J. Phys. C Solid State 16 (17) (1983) L561.
[7] H.A. Harwig, A.G. Gerards, J. Solid State Chem. 26 (3) (1978) 265.
[8] A.F. Gualtieri, S. Immovilli, M. Prudenziati, Powder Diffract. 12 (2) (1997) 90.
[9] A.R. West, Solid State Chemistry and Its Applications, John Wiley & Sons, Inc., Chichester, West Sussex, 2014.
[10] C.D. Ling, J. Solid State Chem. 148 (2) (1999) 380.
[11] W.Z. Zhou, J. Solid State Chem. 108 (2) (1994) 381.
[12] W. Zhou, D.A. Jefferson, J.M. Thomas, P. Roy. Soc. Lond. A Mat. 406 (1831) (1986) 173.
[13] W. Zhou, J. Solid State Chem. 101 (1) (1992) 1.
[14] T. Takahashi, H. Iwahara, J. Appl. Electrochem. 3 (1) (1973) 65.
[15] H.I. Takehiko Takahashi, Takao Esaka, J. Electrochem. Soc. 124 (10) (1977) 1563.
[16] J.A. Switzer, M.G. Shumsky, E.W. Bohannan, Science 284 (5412) (1999) 293.
[17] H.T. Fan, S.S. Pan, X.M. Teng, C. Ye, G.H. Li, J. Phys. D. Appl. Phys. 39 (9) (2006) 1939.
[18] H.T. Fan, S.S. Pan, X.M. Teng, C. Ye, G.H. Li, L.D. Zhang, Thin Solid Films 513 (1–2) (2006) 142.
[19] V. Fruth, M. Popa, D. Berger, R. Ramer, A. Gartner, A. Ciulei, A. Zaharescu, J. Eur. Ceram. Soc. 25 (12) (2005) 2171.
[20] S. Sanna, V. Esposito, J.W. Andreasen, J. Hjelm, W. Zhang, T. Kasama, S.B. Simonsen, M. Christensen, S. Linderoth, N. Pryds, Nat. Mater. 14 (5) (2015) 500.
[21] P. Lunca Popa, S. Sønderby, S. Kerdsongpanya, J. Lu, N. Bonanos, P. Eklund, J. Appl. Phys. 113 (4) (2013) 046101.
[22] A. Helfen, S. Merkourakis, G. Wang, M.G. Walls, E. Roy, K. Yu-Zhang, Y. Leprince-Wang, Solid State Ionics 176 (5–6) (2005) 629.
[23] C.L. Gomez, O. Depablos-Rivera, J.C. Medina, P. Silva-Bermudez, S. Muhl, A. Zeinert, S.E. Rodil, Solid State Ionics 255 (2014) 147.
[24] W.C.J. Wei, Adv. Mater. Res. 51 (2008) 111.
[25] E.D. Wachsman, J. Eur. Ceram. Soc. 24 (6) (2004) 1281.
[26] G.Y. Meng, C.S. Chen, X. Han, P.H. Yang, D.K. Peng, Solid State Ionics 28 (1988) 533.
[27] D.W. Jung, K.L. Duncan, E.D. Wachsman, Acta Mater. 58 (2) (2010) 355.
[28] L.S. Wang, S.A. Barnett, J. Electrochem. Soc. 139 (9) (1992) 2567.
[29] K. Laurent, G. Wang, S. Tusseaunenez, Y. Leprincewang, Solid State Ionics 178 (33–34) (2008) 1735.
[30] S. Sanna, V. Esposito, C. Graves, J. Hjelm, J.W. Andreasen, N. Pryds, Solid State Ionics 266 (2014) 13.
[31] S. Sanna, V. Esposito, M. Christensen, N. Pryds, APL Mater. 4 (12) (2016) 121101.
[32] C.L. Gomez, O. Depablos-Rivera, P. Silva-Bermudez, S. Muhl, A. Zeinert, M. Lejeune, S. Charvet, P. Barroy, E. Camps, S.E. Rodil, Thin Solid Films 578 (2015) 103.
[33] P. Lunca Popa, S. Sønderby, S. Kerdsongpanya, J. Lu, H. Arwin, P. Eklund, Thin Solid Films 624 (2017) 41.
[34] E.W. Bohannan, C.C. Jaynes, M.G. Shumsky, J.K. Barton, J.A. Switzer, Solid State Ionics 131 (1–2) (2000) 97.
[35] N.C. Halder, C.N.J. Wagner, Acta Crystallogr. 20 (2) (1966) 312.
[36] M.G. Bellino, D.G. Lamas, N.E. Walsöe de Reca, Adv. Funct. Mater. 16 (1) (2006) 107.
[37] Y.J. Kang, H.J. Park, G.M. Choi, Solid State Ionics 179 (27–32) (2008) 1602.
[38] A. Tschöpe, E. Sommer, R. Birringer, Solid State Ionics 139 (3–4) (2001) 255.
[39] J.R. Macdonald, Ann. Biomed. Eng. 20 (3) (1992) 289.
[40] J. Ross Macdonald, Impedance Spectroscopy: Emphasizing Solid Materials and Systems, Wiley, 1987.
[41] N. Jiang, E.D. Wachsman, J. Am. Ceram. Soc. 82 (11) (1999) 3057.
[42] S. Boyapati, E.D. Wachsman, N. Jiang, Solid State Ionics 140 (1) (2001) 149.
[43] N. Jiang, E.D. Wachsman, S.-H. Jung, Solid State Ionics 150 (3–4) (2002) 347.
[44] Y. Lee, J.H. Joo, G.M. Choi, Solid State Ionics 249–250 (2013) 165.
[45] D. Virbukas, M. Sriubas, G. Laukaitis, Solid State Ionics 271 (2015) 98.
[46] J.L.M. Rupp, L.J. Gauckler, Solid State Ionics 177 (26–32) (2006) 2513.
[47] T. Suzuki, I. Kosacki, H.U. Anderson, Solid State Ionics 151 (1–4) (2002) 111.
[48] G. Laukaitis, J. Dudonis, A.F. Orliukas, D. Milcius, Solid State Ionics 179 (1–6) (2008) 182.
[49] G. Laukaitis, D. Virbukas, J. Dudonis, O. Katkauskė, D. Milčius, Solid State Ionics 188 (1) (2011) 41.
[50] J.H. Joo, G.M. Choi, Solid State Ionics 177 (11 – 12) (2006) 1053.
[51] P. Shuk, H.D. Wiemhofer, U. Guth, W. Gopel, M. Greenblatt, Solid State Ionics 89 (3–4) (1996) 179.
[52] I. Kosacki, T. Suzuki, V. Petrovsky, H.U. Anderson, Solid State Ionics 136–137 (2000) 1225.
[53] M.G. Bellino, D.G. Lamas, N.E. Walsöe de Reca, Adv. Mater. 18 (22) (2006) 3005.
[54] W. Jung, J.L. Hertz, H.L. Tuller, Acta Mater. 57 (5) (2009) 1399.
[55] N. Sata, K. Eberman, K. Eberl, J. Maier, Nature 408 (6815) (2000) 946.
[56] S. Sanna, V. Esposito, A. Tebano, S. Licoccia, E. Traversa, G. Balestrino, Small 6 (17) (2010) 1863.
[57] N. Pryds, V. Esposito, J. Electroceram. 38 (1) (2017) 1.
[58] D.P. Almond, A.R. West, Solid State Ionics 11 (1) (1983) 57.
[59] A.R. West, D.C. Sinclair, N. Hirose, J. Electroceram. 1 (1) (1997) 65.
[60] A. Orliukas, P. Bohac, K. Sasaki, L.J. Gauckler, Solid State Ionics 72 (1994) 35.
[61] A.F. Orliukas, T. Šalkus, A. Kežionis, V. Venckutė, V. Kazlauskienė, J. Miškinis, G. Laukaitis, J. Dudonis, Solid State Ionics 188 (1) (2011) 36.
[62] R.C. Garvie, J. Phys. Chem. 69 (4) (1965) 1238.
[63] W. Zhou, D.A. Jefferson, J.M. Thomas, J. Solid State Chem. 70 (1) (1987) 129.
[64] D.W. Jung, J.C. Nino, K.L. Duncan, S.R. Bishop, E.D. Wachsman, Ionics 16 (2) (2010) 97.
[65] N.Q. Minh, T. T., Science and Technology of Ceramic Fuel Cells, Elsevier Science B. V., 1995.
[66] D.S. Aidhy, S.B. Sinnott, E.D. Wachsman, S.R. Phillpot, Ionics 16 (4) (2010) 297.
[67] E.D. Wachsman, S. Boyapati, N. Jiang, Ionics 7 (1) (2001) 1.
[68] V. Dimitrov, T. Komatsu, J. Solid State Chem. 196 (2012) 574.
[69] N.W. Kwak, W. Jung, Acta Mater. 108 (2016) 271.
[70] X. Guo, E. Vasco, S. Mi, K. Szot, E. Wachsman, R. Waser, Acta Mater. 53 (19) (2005) 5161.
[71] J. Jiang, J.L. Hertz, J. Mater. Chem. A 2 (45) (2014) 19550.
[72] G. Gregori, M. Shirpour, J. Maier, Adv. Funct. Mater. 23 (47) (2013) 5861.
[73] B. Scherrer, M.V.F. Schlupp, D. Stender, J. Martynczuk, J.G. Grolig, H. Ma, P. Kocher, T. Lippert, M. Prestat, L.J. Gauckler, Adv. Funct. Mater. 23 (15) (2013) 1957.